SHORT THESIS FOR THE DEGREE OF DOCTOR OF PHILOSOPHY (PHD)

Identification and characterization of bacterial metabolites with antineoplastic activity in breast cancer

by Gyula Ujlaki

Supervisor: Prof. Dr. Péter Bay

UNIVERSITY OF DEBRECEN
DOCTORAL SCHOOL OF MOLECULAR MEDICINE

DEBRECEN, 2024

Identification and characterization of bacterial metabolites with antineoplastic activity in breast cancer

By Gyula Ujlaki,
Moecular biologist MSc

Supervisor: Prof. Dr. Péter Bay

Doctoral School of Molecular Medicine,
University of Debrecen

Head of the **Defense Committee**:	Prof. Dr. László Csernoch, DSc
Reviewers:	Dr. Krisztina Köröskényi, PhD
	Dr. Tibor Pankotai, PhD
Members of the Defense Committee:	Dr. István Szatmári, PhD
	Dr. Ágota Apáti, PhD

The PhD Defense takes place at the Lecture Hall of Bldg. A, Department of Internal Medicine, Faculty of Medicine, University of Debrecen at 14:00, 21st of October, 2024.

Introduction

Breast cancer

Malignant tumors are complex systemic diseases that result from multiple cellular and genomic alterations, posing an increasingly severe healthcare problem in Hungary. According to data from the Hungarian National Cancer Registry, in 2020, 7144 new patients were identified with malignant breast tumors.

Among US women, breast cancer is the second leading cause of cancer-related death. Approximately one million cases are diagnosed each year, with an estimated annual mortality of 23.1 deaths per 100,000 persons in Europe. According to the 2019 breast cancer report published by the American Cancer Society, the incidence of breast cancer increased by an average of 0.3% annually between 2012 and 2016. However, the mortality rate has significantly decreased in recent decades due to the widespread adoption of regular screening. In the United States, there were approximately 287,850 newly diagnosed cases of invasive breast cancer and 51,400 newly diagnosed cases of *in situ* breast cancer in 2022. Based on statistical data, it is estimated that 43,250 women were expected to die from breast cancer in the United States in 2022. Breast cancer incidence shows significant geographic and economic disparities, with higher occurrence rates observed in developed countries. Nevertheless, due to the promotion of screening programs and consequently early detection, the five-year survival rate for breast cancer is 99% for *in situ* breast cancer, 86% for breast cancer with regional lymph node metastasis, and 30% for breast cancer with distant metastasis according to the SEER database.

The risk factors for the development of breast cancer are:

- Gender and age,
- Genetic and epigenetic factors, including BRCA1 and BRCA2 gene mutations, high expression of epidermal growth factor receptor (EGFR) and human epidermal growth factor receptor (HER2),
- Prolonged hormone exposure, such as the use of oral contraceptives, hormone replacement therapies, as well as early menarche or late menopause,
- Breast cancer or other neoplastic diseases in the medical history of the family,
- Obesity, regular smoking, and alcohol consumption,

- Dense breast tissue.

In contrast, pregnancy, breastfeeding, regular physical activity, and healthy lifestyle free from harmful addictions can reduce susceptibility to breast cancer.

Sustained proliferation in breast cancer

In normal tissues, the expression of growth-promoting signals is tightly regulated to sustain tissue homeostasis, structure, and function. However, cancer cells acquire the capability to sustain proliferative signals and continuously proliferate beyond their normal lifespan, thereby disrupting the structure of the normal tissue.

Cancer cells can sustain their growth promoting signals through:

- overexpressing growth factor receptors,
- producing their own growth factors (autocrine signaling),
- mutations in the growth factor signaling pathways.

Mutations in growth signaling pathways allow cancer cells to prevent apoptosis, compromise cell cycle exit, or drive cell cycle progression. Gene mutations in growth signaling are frequently occurring in the members of MAPK, PI3K, Akt signaling, and mTOR signaling pathways. These mutations also provide resistance against conventional therapeutic approaches.

Losing growth control mechanisms in neoplastic cells provide them the ability to avoid growth inhibition and elimination by tumor suppression proteins. These tumor suppressor proteins inhibit the proliferation of mutated cells by controlling cell cycle, induce senescence, quiescence or even apoptosis in critically damaged cells. Genetic mutations are not only affecting growth promoting signals, but also occur in tumor suppressor genes at approximately 70% of the cases. The two most important tumor suppressors are the Retinoblastoma protein (Rb) and tumor protein 53 (p53), which are mediating the G0/G1 phase checkpoints of the cell cycle.

The literature on sustained cellular proliferation is vast, therefore, we will focus on those pathways that are important for the interpretation of our results. In breast cancer cell proliferation and growth signaling, the Wnt/β-catenin pathway holds a central position. Mutations leading to the stabilization of β-catenin or β-catenin targets are frequently associated with increased tumor aggressiveness. When the WNT pathway is downregulated, β-catenin is ubiquitinated and phosphorylated by GSK-3β on the destruction complex. This leads to the degradation of β-catenin. Alternatively, when the WNT pathway upregulated, the destruction complex is disrupted, GSK-

3β does not phosphorylate the β-catenin. In this active state, β-catenin translocates to the nucleus, where it induces the expression of *CYCLIN D1, c-MYC, PDK, MTC-1, MMP7*, fibronectin, *COX2* and *AXIN-2* genes. Constitutive β-catenin signaling appears to support the survival and growth of stem cells during the early stages of tumor development. Constitutive activation of the β-catenin pathway is frequently associated with CTNNB1, APC, AXIN-1 and AXIN-2 gene mutations. To assess β-catenin activity, the phosphorylation status of GSK-3α/β is usually assessed, as when GSK-3α/β is phosphorylated (deactivated), it cannot effectively phosphorylate β-catenin, which protects β-catenin from degradation.

EMT in breast cancer

Cells in carcinomas usually lose their epithelial morphology in a process, called epithelial-mesenchymal transition (EMT). EMT is a complex biological process through which epithelial cells undergo a series of molecular changes that result in a transition to a mesenchymal cell phenotype. In general, mesenchymal cells lose their ability for focal adhesion and become mobile. Mobility enables the spreading of cancer and metastasis formation. This process plays a critical role during embryonic development, tissue repair and wound healing, as these cells have the ability to migrate. EMT has been implicated in various pathological conditions, including cancer progression and metastasis.

Epithelial cells undergo EMT in response to signals received from their (micro)environment, or in response to mutations in EMT signaling. Studying EMT is challenging, since cell morphology and molecular characteristics are usually not painting a binary picture, exclusively indicating either epithelial or mesenchymal state. Certain cytokines like transforming growth factor-β (TGF-β), fibroblast growth factor (FGF) family, epidermal growth factor (EGF), and hepatocyte growth factor (HGF) are known to induce or promote the EMT. These EMT-inducing signals up-regulate specific transcription factors, such as SNAI (Snail Family Transcriptional Repressor), TWIST (Twist Family BHLH Transcription Factor), ZEB (Zinc finger E-box binding homeobox), and β-catenin. EMT transcription factors often collaborate with miRNAs and various epigenetic and post-translational regulators to orchestrate EMT control. The miR-34 family is recognized for its role in regulating EMT and suppressing early phases of tumor metastasis. In particular, miR-34a prevents TGF-β induced EMT and regulates SNAI1 expression through its 3'-UTR. It also suppresses SLUG and ZEB1. Carcinoma cells typically exhibit a spectrum of epithelial-

mesenchymal characteristics, among which E-cadherin, occludins, and cytokeratins are commonly used as epithelial markers, while N-cadherin and vimentin are applied as mesenchymal markers. E-cadherin and occludins are located in tight junctions on the surface of epithelial cells, where their main role is to maintain cell-cell connections, while cytokeratins are members of cytoskeletal intermediate filaments and their composition is different when comparing normal and cancerous cells. The mesenchymal marker N-cadherin also mediates cell-cell adhesion, but induce changes in cell behavior in favor of migratory phenotype in EMT. Vimentin is an intermediate filament protein associated with EMT phenotype. Recent research has shown that certain cancer cells express both epithelial and mesenchymal markers, as observed in breast, pancreatic, renal, lung, and colorectal cancers.

Tumor cell energy metabolism

The most prevalent course for pyruvate, the product of glycolysis, involves its conversion through the pyruvate dehydrogenase (PDH) complex into acetyl-coenzyme A. Acetyl-coenzyme A is subsequently transformed to citrate by condensing with oxaloacetate through the action of citrate synthase. Consequently, citrate can either be converted into isocitrate as part of the citric acid (or Krebs) cycle, or it can exit the mitochondria. When citrate leaves the mitochondria, it is metabolized by ATP citrate lyase to produce cytosolic acetyl-coenzyme A. That serves as a substrate for processes, such as *de novo* lipogenesis and protein acetylation. The proper functioning of the pyruvate-citrate shuttle within mitochondria is thus crucial for the synthesis of fatty acids, cholesterol, and protein acylation. With some exceptions, such as in the cases of hypoxia, the primary source of lipogenic acetyl-coenzyme A for most cancer cells originates from glucose-derived pyruvate via the PDH pathway.

Apart from carbohydrates, amino acids play a vital role as substrates that fuel both mitochondrial metabolism and the creation of proteins, lipids, and various other molecules. Particularly in the context of cancer, specific mitochondrial enzymes involved in processing glutamine, proline, aspartate, and alanine are of significant interest. Among these, glutamine holds special importance as a nutrient crucial for cell proliferation. This is due to the fact that the amido nitrogen within this amino acid serves as an essential substrate for generating hexosamine and nucleotides in the cytosol. Moreover, glutamine may serve as an important anaplerotic substrate, contributing to the replenishment of intermediates within the TCA cycle's metabolic processes.

Carbon from glutamine can additionally contribute to the production of acetyl-coenzyme A, which is essential for synthesizing lipids. This process occurs when glutamine undergoes metabolic reactions facilitated by malic enzymes through either glutaminolysis or reductive carboxylation pathways. These malic enzymes are found both in the cytosol and within mitochondria. Tumor cells have the capacity to upregulate the expression of either one or both isoforms of malic enzymes.

Next to amino acids and lipids, nucleotide synthesis is significantly supported by mitochondrial metabolism and its intermediate metabolites. Although the ribose part of nucleotides are exclusively synthesized in the cytoplasm, a number of these intermediate metabolites are necessary for purin and pirimidin base synthesis.

The metabolic changes are associated, with the complex reprogramming of the cellular energy sensor system. Among others, this web of sensors encompass mTOR, forkhead box O1 (FOXO1), adenosine monophosphate-activated protein kinase (AMPK), as well as peroxisome proliferator-activated receptor gamma coactivator-1α and β (PGC-1α and PGC-1β). The induction of mTOR complexes (mTORC1 and mTORC2) enhances the expression and activity of genes involved in the Warburg effect and glutaminolysis. Meanwhile, the FOXO1 transcription factor primarily triggers cell cycle arrest or decreased cell proliferation capacity through the inhibition of mTORC1 leading to tumor suppression. In patients with breast cancer, lower activity of the serine/threonine kinase, AMPK was observed. Low AMPK activity is associated with aerobic glycolysis (Warburg effect) and enhanced tumor growth. The antitumor effect of AMPK plays a crucial role in maintaining energy homeostasis and stimulates mitochondrial biogenesis through the regulation of PGC-1α and PGC-1β. In human breast cancer, the activity of nuclear respiratory factor 1 (NRF1) is upregulated. NRF1 and NRF2 play essential roles in regulating the expression of electron transfer chain subunits encoded by the nuclear genome and in binding to the promoters of genes involved in mitochondrial DNA (mtDNA) transcription. These transcription factors are influenced by transcription coactivators, predominantly by PGC-1α. In breast cancer, therapeutic approaches targeting Warburg-type metabolic rearrangements can reduce the proliferation of cancer cells holding a promise for identifying druggable signaling pathways.

The gut microbiome

The microbiome refers to the assembly of microbial species of a compartment identified through next generation sequencing and subsequent sequence alignment. The microbiome is characterized by the number and the abundance of the species in a compartment. Diversity of the microbiome also extends beyond individual species. It encompasses the genetic diversity within each microbial species, allowing functional versatility and adaptation to changing environments This genetic diversity enables the microbiome to produce a wide range of bioactive compounds, including enzymes and vitamins too, which can have profound effects on human health. Disruptions or imbalances in microbiome composition, known as dysbiosis, is associated with various diseases and conditions.

The diversity of the microbiome is shaped by various factors, such as the individual's age, ethnicity, hormonal levels, and lifestyle choices as diet, prebiotics, probiotics, stress, hygiene, alcohol consumption, smoking habits, antibiotic use, or iatrogenic factors as chemotherapy and radiation. The composition of the microbiome varies significantly from person to person, giving rise to a unique microbial fingerprint for each individual.

Dysbiosis of the gut microbiome in breast cancer

In breast cancer, oncobiotic changes in various microbial compartments occur, including breast tissue, milk ducts, the intrinsic microbiome of breast carcinoma, the distal gut, and the urinary microbiome. Moreover, breast cancer tissue have been found to contain viruses (parapoxviruses, human papillomavirus, Herpesviridae, Retroviridae, Parapoxviridae, Polyomaviridae, Papillomaviridae), fungi, and parasites, though these markers are not consistently found in all individuals. Microbiome signatures within the oncobiome are associated with survival in breast cancer, highlighting the importance of oncobiotic changes. Microbiome is now recognized as a constituent of the tumor microenvironment. Breast cancer risk factors are linked to reduced diversity, high-density breast tissue, early menarche, low physical activity, and increased body mass index (BMI). Additionally, excessive use of antibiotics, which decreases diversity, may increase the risk of breast cancer, whereas probiotics that enhance diversity may have a protective effect.

The gut microbiome and the breast tumor are separated, therefore signaling pathways are required to establish connections between these distant compartments. Numerous pathways

facilitate cross-connections between the microbiome and the tumor tissue. Intestinal bacteria that express β-galactosidases (gus and BG genes) can deconjugete excreted conjugated estrogens. The gus gene is widespread among bacteria, whereas alterations in BG involve *Bacteroidetes* and *Firmicutes*. Several bacteria, including *Collinsella, Edwardsiella, Alistipes, Bacteroides, Bifidobacterium, Citrobacter, Clostridium, Dermabacter, Escherichia, Faecalibacterium, Lactobacillus, Marvinbryantia, Propionibacterium, Roseburia*, and *Tannerella* have been found to express β-glucuronidases. The oncobiome exhibits an increased capacity to reactivate estrogens, enabling their reuptake and promotion of the development of estrogen-dependent breast tumors that express the estrogen receptor (ER+). It is noteworthy that the ability to reactivate estrogen was discovered through analyzing the pathways within the microbiomes of the breast and nipple aspirates.

Metabolites with bioactive properties, produced by either the microbiome or the oncobiome, can act similarly to hormones and establish a link between the microbiome and cancer cells in remote locations. Considering the gut microbiome harbors the largest number of bacteria in the body, its metabolic capacity is significant. However, the biosynthetic capacity of the microbiome is suppressed relative to the eubiome. Several bioactive bacterial metabolites have been discovered that can influence the behavior of breast cancer cells. These metabolites include cadaverine, secondary bile acids, indole metabolites, and short-chain fatty acids (SCFAs). Notably, these metabolites modulate different processes in carcinogenesis, such as cell proliferation, EMT and oxidative stress. Studies have also revealed that the metabolic capacity of the gut microbiome is suppressed in breast cancer, resulting in a reduction in the production of well-known antineoplastic metabolites.

Secondary bile acid biosynthesis and reabsorption

Bile acids are important molecules involved in the digestion and dietary fat absorption. The liver synthesizes around 200-600 mg of primary bile acid daily from cholesterol. These primary bile acids are the cholic acid and chenodeoxycholic acid. About 5% of the total bile acid pool is eliminated through stool each day, while the rest is reabsorbed at the terminal ileum and enters the enterohepatic circulation. The total bile acid quantity is approximately 3 g. The synthesis of primary bile acids from cholesterol involves the activity of 17 different enzymes located in different cellular compartments, including the cytoplasm, endoplasmic reticulum, mitochondria,

and peroxisomes. The key initial reaction in the classic transformation is catalyzed by cholesterol 7α-hydroxylase (CYP7A1), which is the rate-limiting step in bile acid synthesis. The presence of sterol 12α-hydroxylase (CYP8B1) during the synthesis results in the end product cholic acid, while its absence leads to the formation of chenodeoxycholic acid. On the alternate pathway, sterol 27-hydroxylase (CYP27A1), a mitochondrial cytochrome P450 enzyme expressed in various tissues, catalyzes the first reaction. However, in the liver, only 9% of the synthesized bile acids are formed via this alternative pathway. After synthesis, the carboxyl group of most bile acids is conjugated with either glycine or taurine. In the distal ileum, conjugated cholic and chenodeoxycholic acids undergo deconjugation, and bacterial 7α-hydroxylases transform them into secondary bile acids, as deoxycholic acid (DCA) and lithocholic (LCA) respectively. Furthermore, bacterial epimerases facilitate the conversion of chenodeoxycholic acid's 7α-hydroxy group to a 7β-hydroxyl group, yielding ursodeoxycholic acid (UDCA). Bacterial enzymes involved in secondary bile acid production are assembled in the bile acid inducible (bai) operon. Transformations of bile acids result in the hydrophobic nature of secondary bile acids, causing them to lose their capability to function as detergents or toxins against bacteria. Subsequently, bile acids are reabsorbed at the terminal ileum and enter the enterohepatic circulation, where they recirculate to the liver. However, a small portion of bile acids bypasses the liver and remains in the systemic circulation, allowing them to reach distant parts of the body through the bloodstream.

Dysregulation in bile acid metabolism and signaling is implicated in various types of cancer. Certain bile acids, particularly secondary bile acids, can have tumor-promoting effects. They can activate signaling pathways involved in cell proliferation, survival, and inflammation. Bile acids can also promote DNA damage and genomic instability, contributing to the initiation and progression of cancer. Bile acids can also interact with specific receptors, such as farnesoid X receptor (FXR) and the G-protein-coupled bile acid receptor 1 (TGR5), which are expressed in various tissues including the liver, intestine and colon. Activation of these receptors by bile acids can modulate gene expression and cellular responses that influence cancer development. On the other hand, some studies suggest that certain bile acids may have anti-cancer properties. For example, UDCA has been investigated for its potential to inhibit cell proliferation and induce apoptosis in liver cancer cells.

The gut microbiome also plays a role in bile acid metabolism, and alterations in the gut microbial composition can impact bile acid profiles. The relation between bile acids and microbial

composition is not unidirectional; bile acids also influence the composition of the gut microbiome. The impact of bile acids on the gut microbiome is likely the result of altering the quorum sensing system in bacteria. Quorum sensing is a mechanism that controls the activation of genes in response to changes in the number of cells within a population. Bacteria are engaged in the quorum sensing produce and release chemical signal molecules known as autoinducers, which accumulate as the cell population grows. When the concentration of these autoinducers reaches a specific threshold, it triggers changes in gene expression. Both Gram-positive and Gram-negative bacteria employ quorum sensing communication systems to regulate wide range of biological processes, including virulence, competence, conjugation, antibiotic synthesis, movement, sporulation, and formation of biofilms. In this regard, bile acids may be implicated in quorum sensing, as they influence the composition of the gut microbiome.

The intestinal microbiome plays a crucial role in the conversion of primary bile acids into secondary bile acids. As a result, the changes caused by secondary bile acids directly implicate the involvement of the intestinal microbiome. In our investigation, we focused on three major secondary bile acids – LCA, DCA, and UDCA. During our experiments, we used secondary bile acids in a specific concentration range representing the secondary bile acids in the serum (LCA: 31 nM, DCA: 701 nM, UDCA: 147 nM), and in breast cyst fluid (LCA: 9-23 µM, DCA: 17-160 µM).

Convolutional neural networks in image analysis

Detecting objects – like the detection of nuclei in a large set of images – with conventional segmentation methods requires readjustment of segmentation parameters between datasets. This could lead to analysis errors between datasets – e.g., wrongly adjusted detection parameters lead to detection of staining artefacts, while leaving faint but valid signals undetected. In the last decade, convolutional neural networks (CNNs) solved this problem in image analysis and by using semantic segmentation models, segmentation of high throughput microscopy images can be standardized between individual datasets as well.

CNNs have been used for computer vision tasks for many years. However, their true potential was not fully realized until the ImageNet competition in 2012, where their efficiency was showcased by harnessing the power of graphics processing units (GPUs), rectified linear unit activation, dropout regularization, and effective data augmentation. CNNs have gained popularity

not only among computer vision experts, but also in various applications such as processing natural language, analysis of hyperspectral images, and medical image analysis. The primary strength of CNNs lies in their deep architecture, enabling the extraction of distinctive features at multiple levels of abstraction. Nevertheless, the full training of a deep CNN from scratch presents challenges. Firstly, CNNs demand a substantial amount of labeled training data, which is a challenge often encountered in the medical field, where obtaining expert annotations can be costly. Secondly, deep CNN training requires considerable computational and memory resources; otherwise, the process becomes excessively time-consuming. Thirdly, overfitting and convergence issues often complicate the training of a deep CNN, necessitating iterative adjustments in the network's architecture or learning parameters to guarantee uniform learning across all layers. As a result, deep learning from scratch can be laborious, time-consuming, and demands considerable expertise and patience. An encouraging option besides training a CNN from the ground up is fine-tuning a pre-trained CNN that has been trained on a large, labeled dataset from a different application. Pre-trained models have been successfully applied in various computer vision tasks as feature generators or as baselines for transfer learning.

An essential characteristic of CNNs lies in the "transferability" of knowledge embedded within pre-trained CNNs. Research indicates that the effectiveness of knowledge transfer relies on the gap or dissimilarity between the dataset used for training a CNN and the target database for knowledge transfer. Although natural image databases and medical imaging databases differ considerably, recent research shows promising potential for knowledge transfer to the medical imaging domain. An application method of transfer learning involves using a pre-trained CNN as a feature generator. In this approach, the pre-trained CNN is utilized on an input image, and the CNN generates (extracts) features from a particular layer of the network. These extracted features are then used to train a new pattern classifier, also known as the output layer of a CNN.

Certain visual tasks, especially in biomedical image processing (e.g., nuclei segmentation), the desired output should involve localization, meaning that a class label needs to be assigned to each pixel in the image. Moreover, obtaining thousands of training images is often challenging in biomedical tasks. To address these issues, a sliding-window setup is adopted to train a network, where the goal was to predict the class label of each pixel by providing a local region (patch) around that pixel as input. This approach has two advantages. Firstly, the network can achieve localization. Secondly, the training data in the form of patches is significantly larger than the

number of training images. However, this strategy has two drawbacks as well. It is relatively slow since the network needs to be run separately for each patch, and there is redundancy due to overlapping patches. Then, there is a trade-off between localization accuracy and the use of context. Larger patches allow for more context information but may reduce localization accuracy due to additional max-pooling layers. Conversely, smaller patches enable better localization accuracy but provide limited context information. More recent approaches have proposed classifier outputs that consider features from multiple layers, enabling good localization while using context effectively. This method of classifying each pixel on an image is called semantic segmentation.

In biomedical image analysis, semantic segmentation with CNNs have found applications beyond computer-aided detection systems. Recent uses include carotid intima-media thickness measurement in ultrasound images, pancreas segmentation in CT images, brain tumor segmentation in MRI scans, multimodality isointense infant brain image segmentation, knee cartilage segmentation in MRI scans, and many applications beyond the scope of this short overview. During the past decade, several popular semantic segmentation models have emerged in the field of biomedical image segmentation:

- UNet stands out as one of the pioneers in biomedical image segmentation, and the model encompasses a symmetric encoder-decoder structure with skip connections.
- DeepLab is utilizing “atrous” convolutions for multi-scale contextual information.
- Mask R-CNN was initially designed for instance segmentation but it’s adaptation to semantic segmentation is also widely applied.
- PSPNet: Pyramid Scene Parsing Network was introduced in 2016, designed to capture multi-scale contextual information in an efficient manner.
- FCN: Fully Convolutional Network is based on an encoder-decoder structure, and widely adopted and adapted for different applications, including biomedical image segmentation.
- LinkNet: It is a lightweight architecture designed for semantic segmentation tasks, and it has gained popularity due to its computational efficiency and effectiveness.

The aims of the study

The dysbiosis of the gastrointestinal microbiome can be associated with various diseases, including the development of breast tumors. We set out to identify and characterize bacterial metabolites, synthesized by the gut microbiome that can reach breast tumor cells through the bloodstream and alter the signaling pathways of the tumor cells to modulate cell proliferation and EMT. According to this, our aims were the following:

1. To assess the cytostatic effects of LCA.
2. To assess the effects of LCA on EMT.
3. To assess the effects of LCA on cellular energy metabolism.
4. To determine the receptor responsible for the effects of LCA.
5. To construct a library of bacterial metabolites with possible antineoplastic effects.
6. To establish high content screening-based methods for the assessment of cell proliferation and EMT.
7. To identify cytostatic bacterial metabolites using the metabolite library.
8. To identify bacterial metabolites affecting EMT.

Materials and Methods

Cell culture

Cell lines were maintained at 37 °C with 5% CO_2. The study employed various cell lines as representative models, including 4T1 murine breast cancer, MCF7 human breast cancer, SKBR3 human breast cancer, A2780 human ovarian cancer, and Capan2 human pancreatic adenocarcinoma cell lines, and also primary fibroblast cells. Exact composition of culture media is specified in **Table 1**.

Table 2. Cell culturing media mixtures.

Cell line	Medium	Reference number	FBS	Penicillin-Streptomycin, (v/v%)	L-glutamine	HEPES	Pyruvate (v/v%)
4T1	RPMI-1640	Sigma R5886	10 %	1 % (P: 100 000U/L, S: 10 mg/l)	2 mM	-	1 % (1 mM)
A2780	RPMI-1640	Sigma R5886	10 %	1 % (P: 100 000U/L, S: 10 mg/l	2 mM	-	-
MCF7	MEM	Sigma M8042	10 %	1 % (P: 100 000U/L, S: 10 mg/l	2 mM	-	-
Capan2	MEM	Sigma M8042	10 %	1 % (P: 100 000U/L, S: 10 mg/l	2 mM	-	-
SKBR3	MEM	Sigma D6429	10 %	1 % (P: 100 000U/L, S: 10 mg/l	2 mM	10 mM	-
Primary fibroblasts	DMEM low glucose	Sigma D5546	20%	1 % (P: 100 000U/L, S: 10 mg/l	2 mM	10 mM	-

Chemicals

Cambridge Isotope Laboratories (Andover, MA, USA) provided the ^{13}C labeled substrates used in the pulse-chase metabolomics experiment. The inhibitors and antagonists used in the TGR5 experiments (U73343 (phospholipase C inhibitor), NF449 (Gsα-selective antagonist), CINPA1 (CAR antagonist), DY268 (FXR antagonist), GSK2033 (LXR antagonist) were obtained from Tocris Bioscience and were applied at a concentration of 5 µM, with the exception of U73343, which was used at a final concentration of 1 µM.

Sulphorhodamine B (SRB) cell proliferation assay

SRB proliferation assay for measuring effects of secondary bile acids

For the assessment of cell proliferation, we used the SRB assay. Cells were seeded on 96-well plates (3000-5000 cells/well). Cells were treated with secondary bile acids for 48 hours. Then cells were fixed with 10% trichloroacetic acid (TCA) and stained with SRB solution (0.4% in 1% acetic acid). Unbound dye was removed by washing with 1% acetic acid. Bound dye was solubilized with 10 mM TRIS base. Absorbance was read on an automated plate reader (Thermo Labsystems Multiskan MS, Thermo Fisher Scientific, Waltham, MA, USA) at 540 nm.

SRB proliferation assay for validating image analysis-based cell proliferation assay

Cells were seeded on 96-well tissue culture test plates and fixed after 8 hours. In parallel to this, cells were also seeded on 96-well high content imaging microplates in the same manner. Cells on tissue culture test plates were fixed with 10% TCA and stained with SRB solution. Unbound dye was removed by washing with 1% acetic acid. Bound dye was solubilized with 10 mM TRIS base. Absorbance was read on an automated plate reader (Thermo Labsystems Multiskan MS) at 540 nm.

Cells on high content imaging microplates were fixed with 4% paraformaldehyde (PFA), then permeabilized with 1% Triton-X 100/PBS solution, unspecific binding sites were blocked with 1% BSA/PBS solution. Nuclei were stained with 4’6-diamidino-2-phenylindole (DAPI). Imaging was made with PerkinElmer Opera Phenix High Content Screening System.

Colony forming assay

In the colony formation assays, a total of 500 cells were initially seeded in each well of a 6-well plate, containing complete growth medium. These cells were then cultured for 7 days in the presence of varying concentrations of LCA, as indicated. After the assay period, the plates were washed twice with PBS. Next, the colonies were fixed in methanol for 15 minutes, followed by drying and staining with May-Grünwald-Giemsa stain for another 15 minutes. Subsequently, the plate was washed with water, and the colonies were quantified using ImageJ software.

DNA and mRNA preparation and quantitation

Total RNA from cells and tumor samples were prepared using TRIzol reagent (Invitrogen Corporation, Carlsbad, CA, USA). For the assessment of the expression of individual genes, two micrograms of RNA were reverse transcribed using High Capacity cDNA Reverse Transcription Kit (Applied Biosystems, Foster City, CA, USA). The qPCR reactions were performed with qPCRBIO SyGreen Lo-ROX Supermix (PCR Biosystems Ltd., London, UK) on Light-Cycler 480 Detection System (Roche Applied Science). Geometric mean of 36B4 and cyclophylin was used for normalization. Primers are listed in **Table 2**.

Table 2. Primers used in the RT-qPCR reactions**.**

Gene symbol	Murine forward and reverse primer (5′-3′)	Human forward and reverse primer (5′-3′)
Atp5g1	GCTGCTTGAGAGATGGGTTC AGTTGGTGTGGCTGGATCA	CTAAACAGCCTTCCTACAGCAACTT TGAACCAGCCACACCAACTGT
Ndufb5	CTTCGAACTTCCTGCTCCTT GGCCCTGAAAAGAACTACG	GTATTCATTGGTCAAGCTGAACTAG CAGCTCCTTTACCCGTAATTCAGC
Cytc	TCCATCAGGGTATCCTCTCC GGAGGCAAGCATAAGACTGG	TAAGAACAAAGGCATCATCTGG AGGCAGTGGCCAATTATTACTC
36b4	AGATTCGGGATATGCTGTTGG AAAGCCTGGAAGAAGGAGGTC	CCATTGAAATCCTGAGTGATGTG GTCGAACACCTGCTGGATGAC
Cyclophilin	TGGAGAGCACCAAGACAGACA TGCCGGAGTCGACAATGAT	GTCTCCTTTGAGCTGTTTGCAGAC CTTGCCACCAGTGCCATTATG

SDS-PAGE and Western blotting

Cells were lysed in RIPA buffer (50 mM Tris, 150 mM NaCl, 0.1% SDS, 1% Nonidet P-40, 1 mM Na_3VO_4, 1 mM NaF, 0.5% sodium deoxycholate, 1 mM phenylmethylsulfonyl fluoride, protease inhibitor mixture, pH 8.0), then boiled with 50 mM Tris, 2% (w/v) SDS, 3.34% (v/v) glycerol, 16,67 mM β-mercaptoethanol. Protein lysates were separated by SDS-PAGE on 10% acrylamide gels and transferred onto a nitrocellulose membrane (Bio-Rad Laboratories, Supported, Hercules, CA, USA). Antibodies were diluted in 5% BSA solution and are shown in **Table 4**. The secondary antibody was anti-rabbit IgG HRP-linked Antibody (Cell Signaling Technology, Danvers, MA, USA). Labelled proteins were detected by a Chemidoc Touch Imaging System using Supersignal West Pico and Supersignal West Femto ECL Kit (Thermo Fisher Scientific). Blots were quantified by densitometry using Image Lab (Bio-Rad) software.

Table 4. Antibodies used in the study

Antibody/die	Concentration	Vendor
Phospho-ACC (Ser79)	1:1000	Cell Signaling Technology (#3661)
Phospho-AMPKα (Thr172)	1:1000	Cell Signaling Technology (#2531)
NRF1	1:1000 (WB) 1:100 (immunocytochemistry)	Abcam (ab175932)
PGC1β	1:1000	Abcam (ab176328)
FOXO1	1:1000	Cell Signaling Technology (#9454)
Phospho-GSK-3α/β (Ser21/9) (D17D2)	1:2000	Cell Signaling Technology (#8566)
GSK-3α/β (D75D3)	1:2000	Cell Signaling Technology (#5676)
β-Catenin	1:1000	Sigma (C7082)
TGR5/GPBAR1	1:1000	NOVUS (NBP2–23669)
TexasRed-X Phalloidin	1:150	Life Technologies (T7471)
SnaiI	1:1000	Cell Signaling Technology (3879S)
Vimentin	1:1000	Cell Signaling Technology (5741S)
β-actin	1:20 000	Sigma (A3854)

Detection of cell death

The assessment of LCA-induced cytotoxicity was conducted using propidium iodide (PI) uptake as an indicator. For the experiment, cells were seeded in 6-well plates (MCF7 – 200 000 cells/well; 4T1 – 75 000 cells/well) and treated with LCA for two days. Subsequently, the cells were stained with 100 µg/mL of propidium iodide (PI) for 30 minutes at 37 °C, washed once with PBS and analyzed using flow cytometry (FACS Calibur, BD Biosciences, San Jose, CA, USA).

Electric cell-substrate impedance sensing (ECIS)

The electric cell-substrate impedance sensing (ECIS) model Zθ by Applied BioPhysics Inc. (Troy, NY, USA) was utilized to monitor the transcellular electric resistance of MCF7 and 4T1

cells, which were seeded (MCF7 – 40 000 cells/well; 4T1 – 20 000 cells/well) on type 8W10E arrays. After 20 hours, the cells were treated with either vehicle or 0.3 μM LCA, and total impedance values were subsequently measured for an additional 48 hours. Multifrequency measurements were taken at 62.5, 125, 250, 500, 1 000, 2 000, 4 000, 8 000, 16 000, 32 000, and 64 000 Hz. The ECIS modeling tool was employed to assess the barrier resistance values of each well at fixed 180s intervals. The reference well was designated as a no-cell control with complete medium.

Metabolomics, pulse-chase metabolomics

Cells treated with LCA were collected after 48 hours of treatment. Following rapid freezing in liquid nitrogen, the labeled cells (cultured in D5030 medium with 10 mM [U-^{13}C]-glucose or [2-^{13}C]-acetate (Cambridge Isotope Laboratories, Andover, MA, USA) and unlabeled cells were extracted using a methanol-chloroform-H_2O solution at 4 °C. The resulting supernatant was separated through centrifugation (15 000g for 10 minutes at 4 °C) and stored at -80 °C for later analysis. The samples were then dried and sonicated in a solution of 3-nitrobenzyl alcohol-trimethyl-chlorosilane, followed by incubation at 80 °C. The reaction was halted by adding ammonium bicarbonate. Subsequently, the samples were diluted with an acetonitrile-water solution, and the derivative metabolites were separated using reversed-phase chromatography in Waters Acquity LC system. To conduct measurements, a Waters Micromass Quattro Micro triple quadrupole mass spectrometer (Waters Corporation, Milford, MA, USA) was employed, operated with an electrospray source in positive ion mode.

Cytochemistry

Immunocytochemistry in secondary bile acid experiments

Cells were grown on coverslips, which were subsequently washed with PBS. The cells were then fixed using 4% PFA for 15 minutes and permeabilized with 1% Triton-X-100 for 5 minutes. Following this, the samples were blocked with 1% BSA for 1 hour and incubated with TexasRed-X Phalloidin (Invitrogen, Oregon, USA) for 45 minutes to analyze cellular morphology. For the cellular localization of the NRF1 protein, the samples were incubated overnight with the NRF1 primary antibody at 4 °C. After washing, the samples were exposed to the secondary antibody

(1:600, anti-rabbit Alexa 488, Life Technologies) for 1 hour at room temperature. TO-PRO-3 iodide (1:1000, Life Technologies) was used to visualize nuclei. The coverslips were rinsed and mounted in Mowiol/Dabco solution. Confocal images were acquired using a Leica SP8 confocal microscopa and LAS AF v3.1.3. software.

Cytochemistry for bacterial metabolite library screening experiments

96-well high content imaging microplates were used for culturing the cells until they reached 70% confluency. The samples were fixed with 4% PFA for 15 minutes, permeabilized using 1% Triton-X 100, and then blocked with 1% BSA/PBS solution. DAPI (Thermo, Cat. No. R3706) was applied to label the nuclei for 5 minutes, while TexasRed-X Phalloidin (Thermo, T7471) was used to label actin filaments for 1 hour. Fluorescent images of the nuclei were captured at 1080x1080 image resolution, using a 10x objective (N.A. 0.3, 1.196 μm/px). DAPI signals (excitation/emission λ: 405/456) were detected across the entire well, encompassing 21 fields. Morphology images (fluorescent pictures of phalloidin-stained cells) were acquired at 2160x2160 pixel image resolution, with a 20x objective (N.A. 0.4, 0.299 μm/px). DAPI and TexasRed-X Phalloidin signals (excitation/emission λ: 561/599) were detected, covering 25 fields in each well. Both sets of images were acquired using the PerkinElmer Opera Phenix High Content Screening System.

Image analysis in metabolite library screening

Deep learning training dataset – nuclei segmentation

A training dataset was generated from a database of DAPI-stained images of A2780 human ovarian cancer cell line, 4T1 mouse breast cancer cell line, Capan2 human pancreatic cancer cell line, and MCF7 human breast cancer cell line. From our image database, 82 images were selected and used as a training dataset. The selection of these images aimed to provide the highest possible variation both within a single image and between images. Criteria for selecting good examples included images with 1) relatively high or low fluorescent signals, 2) staining errors or artefacts, or 3) overconfluent nuclei with mixed nuclear morphology that covered part of the well edge. First, nuclei were segmented using CellProfiler (Broad Institute, Cambridge, MA, USA) and subsequently, manual corrections were applied. The original dataset underwent augmentation

using the Albumentations (Python3) library, incorporating rotation by 90°, cropping, and brightness changes. As a result, 277 pairs of gray-scale images and the corresponding segmented images were obtained. The order of images in the augmented dataset was randomized, and the dataset was divided into training, test, and validation sets in a 80:10:10 ratio.

Training parameters for deep learning

On the prepared DAPI dataset, a VGG-UNet semantic segmentation model was trained. The model's architecture was extracted from Keras-segmentation 0.3.0 library (Python3). The model was trained on central processing unit (CPU) for 2 epochs, 8 images per batch through 33 steps. The model used for evaluating the model experimental data, had a loss value of 0.0512 and an accuracy value of 0.9874 on the validation dataset.

Nuclei counting proliferation assay

CellProfiler's integrated object segmentation method (adaptive Otsu method with three classes – middle class assigned to background) was employed to segment the nuclei (https://cellprofiler.org/, version 3.1.8.). Subsequently, the object number on each image was counted. In parallel, the trained semantic segmentation model was applied to replace CellProfiler's segmentation method, and then the objects were counted using CellProfiler.

Cell Morphology analysis

The acquired morphology images were segmented and analyzed using Harmony 4.8 software. First, nuclei and cytoplasms were segmented, and then properties of texture, signal intensity, and position of the segmented objects were calculated. Subsequently, a linear regression model was trained with the calculated morphological properties of TGF-β treated, SB-431542 treated, and control cells to classify the cells into either epithelial or mesenchymal morphology groups.

Animal experiments, infiltration score, and TIL calculation

All animal experiments were authorized by the local and national ethical board (reg. 1/2015/DEMÁB) and were performed to conform the relevant EU and US guidelines. Experimental animals were female BALB/c mice between 8 and 10 weeks of age (20-25g).

Animals were bred in the "specific pathogen free" zone of the Animal Facility at the University of Debrecen, and kept in the "minimal disease" zone during the experiment. Animal studies are reported in compliance with the ARRIVE guidelines.

Tissue samples were collected from BALB/c mice grafted with 4T1 breast cancer cells in the *in vivo* experiments. Tumor infiltrating lymphocyte (TIL) content was counted in sections of HE-stained, formalin-fixed, paraffin embedded tumor tissues as the number of TILs per 100 tumor cells.

Bacterial metabolite screening library

TGF-β1 was acquired from Thermo Scientific (Ref.: #100.21), SB-431542 was acquired from Sigma (St. Louise, MO, USA, Ref.: S4317). Source, applied concentrations, and reference serum concentration of each metabolite is provided in **Table 5**.

Table 5. Specifications of the bacterial metabolites

Metabolite name	Solvent	Reference number	Serum reference concentrations (µM)	Applied concentrations (µM)
1-Butanol	PBS	Sigma B7906-500ML	0 - 0.27 [160]	0.005 , 0.015 , 0.044 , 0.13 , 0.4
1-Propanol	PBS	Sigma 96566-5ML-F	0 - 0.8 [160]	0.05 , 0.1 , 0.2 , 0.4, 0.8
2,3 butanediol	PBS	Sigma B84904	0.5 - 0.9 [161]	0.48, 0.56, 0.66, 0.77, 0.9
3,4-dihydroxyphenyl acetic acid	PBS	Sigma 850217-14	0.0102 - 0.104 [162], [163]	0.01, 0.018, 0.032, 0.058, 0.104
3-Hydroxyphenylacetic acid	PBS	Sigma H49901	0.11 - 0.174 [162]	0.106, 0.120, 0.136, 0.154, 0.174
3-Hydroxypropionic acid	PBS	Sigma 792659-1G	3, 6, 8 (individual values) [164]	0.5 , 1 , 2 , 4 , 8
4-aminobenzoic acid	EtOH	Sigma A9878-5G	5.01 - 32.0 [165]	0.3, 1.2, 3.6, 10.8, 32.4
4-hydroxybenzoic acid	PBS	Sigma 8218140250	0.019 - 0.035 [162]	0.019, 0.022, 0.026, 0.03, 0.035

Metabolite name	Solvent	Reference number	Serum reference concentrations (µM)	Applied concentrations (µM)
4-Hydroxyphenylacetic acid	PBS	Sigma H50004-54	0.283 - 0.61 [162]	0.28, 0.36, 0.41, 0.5, 0.61
Acetic acid	PBS	VWR UN2789	23 - 254.4 [160], [166]–[169]	15, 30, 60, 120, 240
Allantoin	DMSO	Sigma 05670	1.0 - 24.0 [170]–[172]	0.99, 2.2, 4.9, 10.8, 24
Butyric acid	PBS	Sigma B103500-5ML	1.39 - 14.15 [166], [167], [169]	1, 2, 4, 8, 16
D-alanine	PBS	Sigma A7377-5G	0 - 0.77 [173]	0.048, 0.96, 0.193, 0.385, 0.77
D-glutamic acid	PBS	Sigma G1001-1G	7.42 - 14.6 [173]	7.28, 8.66, 10.31, 12.27, 14.6
D-mannitol	PBS	Sigma M4125-10MG	no report, same concentrations as for D-mannose	6.25, 12.5, 25, 50, 100
D-mannose	DMSO	no data	13 - 73.87 [174]–[176]	6.25, 12.5, 25, 50, 100
Ethylene glycol	PBS	no data	no data, toxic (1.56 mg/kg)	1, 3, 9,27, 81
Formic acid	PBS	Sigma F0507-500ml	11.84 - 224.5 [177]	10, 30, 90, 270, 810
Glycolic acid	PBS	Sigma 124737	6.1 – 69 [164], [178]	1, 3, 9,27, 81
Hippuric acid	PBS	Sigma 112003	1.5 - 21.2 [162], [179]	0.024, 0.12, 0.6, 3, 15
Hydrocinnamic acid	EtOH	Sigma 135232-5G	0.131 - 0.354 [180]	0.128, 0.165, 0.213, 0.274, 0.354
Isobutyric acid	PBS	Sigma I1754-100ML	1.02 - 14.15 [166], [169]	1.02, 1.97, 3.80, 7.33, 14.15
L-pipecolic acid	PBS	Sigma P2519	1.2 - 3.72 [181]	0.25, 0.5, 1, 2, 4
oxalic acid	PBS	Sigma 75688	6.5 - 35.5 [182], [183]	6.5, 9.9, 15.2, 23.2, 35.5
Propionic acid	PBS	Sigma P1386-1L	4.86 - 15.33 [166], [167], [169]	1.25, 2.5, 5, 10, 20

Metabolite name	Solvent	Reference number	Serum reference concentrations (µM)	Applied concentrations (µM)
Shikimic acid	DMSO	Sigma S5375-10MG	0.03 - 0.23 [184]	0.01, 0.03, 0.09, 0.27, 0.81
trans-ferulic acid	DMSO	Sigma 52229	0.04 - 15.7 [162], [179]	0.016, 0.08, 0.4, 2, 10
Trimethylamine (TMA)	PBS	Sigma 92260	0.3 -14.44 [185], [186]	0.3, 0.79, 2.1, 5.4, 14.35
Trimethylamine-N-oxide (TMAO)	PBS	Sigma 317594	1.21 - 21.1 [187]–[189]	1.22, 2.48, 5.065, 10.33, 21.1
Vanillic acid	PBS	Sigma H36001	0.01 - 0.338 [162], [179]	0.01, 0.024, 0.058, 0.140,0.338

Statistical analysis

Unless stated otherwise, the comparison of two groups was conducted using a two-tailed Student's t-test. To achieve normal distribution in the LCA experiments, the fold data were log_2 transformed. For multiple comparisons, a one-way analysis of variance test (ANOVA) was employed, followed by Tukey's honestly significant difference (HSD) post-hoc test. The data is presented as average ± SD unless stated otherwise. Outliers for LCA experiments were identified using Thomson tau-test, while outliers in other cases were identified using the Z-score test. The statistical analysis was performed using GraphPad Prism v8.0.

Results

Lithocholic acid attenuates aggressivity of breast cancer

Lithocholic acid inhibits cell proliferation.

In the first phase of our study, we performed short-term proliferation assays to assess the impact of secondary bile acids on cell proliferation. LCA reduced cellular proliferation in MCF7, SKBR3 and 4T1 breast cancer cells within the concentration range of 10 nM to 10 μM, that encompassed the reference concentration range of LCA in serum (31 nM) and breast cyst fluid (9-23 uM). This effect was specific to cancer cells, as primary fibroblasts showed no response to LCA at the same concentrations.

Conversely, other secondary bile acids, namely DCA and UDCA, did not exhibit any significant effect on the proliferation of MCF7 and 4T1 breast cancer cells. These findings suggest that the impact of secondary bile acids on breast cancer cell proliferation is not uniform among different types of secondary bile acids.

The cytostatic effect of LCA was validated in colony forming assays. While our investigation revealed a notable reduction in cell proliferation in response to LCA treatment, it was also possible that this decline could be influenced by cell death. To assess this aspect, we performed a propidium iodide assay, which allowed us to examine cell death. The results of this assay demonstrated that the number of propidium iodide positive cells did not exhibit any significant increase upon exposure to LCA. This outcome was consistently observed across both the 4T1 and MCF7 cell lines.

LCA impact on EMT and metastasis

Next, we investigated the potential of LCA to modulate epithelial-mesenchymal transition (EMT). LCA treatment shifted cellular morphology towards an epithelial-like phenotype. This phenomenon was consistently present both in MCF7 and 4T1 cell lines. ECIS measurements showed increased total impedance, providing functional evidence of improved cell-to surface and cell-to-cell adhesion. Upon LCA treatment in scratch assay experiments, a notable reduction in migration speed towards the void area was evident in case of 4T1 cell line.

Additionally, LCA treatment hindered β-catenin signaling, evidenced by decreased phosphorylation of GSK-3α and GSK-3β, as well as reduced β-catenin protein content in both cell lines and *in vivo*.

LCA treatment also resulted in lower VEGF mRNA expression, and a higher number of tumor-infiltrating lymphocytes (TILs) in mice treated with LCA compared to vehicle-treated mice.

LCA affects energy metabolism

Warburg metabolism, a hallmark of cancer, has emerged as a prominent metabolic alteration in breast cancer. In this context, breast cancer cells generally display a characteristic shift towards a glycolytic phenotype, wherein they preferentially rely on glycolysis to produce energy under aerobic conditions. Thus, we examined the impact of LCA on cellular metabolism. Treatment with LCA led to an increase in glycolysis (extracellular acidification rate -ECAR) and mitochondrial respiration (oxygen consumption rate – OCR) levels. Consistently, intracellular lactate and citrate levels, along with the citrate/lactate ratio, were elevated upon LCA treatment.

Moreover, LCA treatment induced the expression of a specific set of OXPHOS genes in both 4T1 and MCF7 cells, aligning with these observations. Next, we conducted pulse-chase metabolomics experiments on MCF7 and 4T1 cells treated with 300 nM LCA. Upon loading the cells with ^{13}C-acetate, a metabolite that can fuel the TCA cycle, LCA treatment resulted in an augmented incorporation of ^{13}C into succinate and malate, indicating an increased flux through the TCA cycle. Additionally, when cells were supplied with ^{13}C-glucose, where ^{13}C atoms enter glycolysis and subsequently fuel the TCA cycle or form lactate, LCA treatment enhanced the levels of ^{13}C-labeled citrate and lactate in MCF7 cells and ^{13}C-labeled succinate and lactate in 4T1 cells. Consistently, the ratio between ^{13}C-citrate and ^{13}C-lactate or between ^{13}C-succinate and ^{13}C-lactate increased, providing further evidence of the mitochondrial dominance in the LCA-induced metabolic switching. We further examined the distribution of 13C-labeled carbons in citrate of MCF7 cells treated with vehicle or LCA. Collectively, these findings indicate that LCA treatment induces activation of the TCA cycle and oxidative phosphorylation (OXPHOS) in breast cancer cells.

To investigate the underlying mechanisms behind the observed metabolic changes, we examined various components of the cellular energy sensor network and mitochondrial transcriptional regulators. Notably, LCA treatment resulted in increased expression and activation

of positive regulators of mitochondrial oxidative phosphorylation, including FOXO1, PGC-1β, and nuclear respirator factor-1 (NRF1). Furthermore, LCA not only elevated their expression but also enhanced their activation, as evidenced by the augmented nuclear translocation of NRF1 and increased phosphorylation of ACC. In our *in vivo* experiments, we also observed that LCA treatment induced AMPK activity, as indicated by elevated levels of phospho-ACC and phospho-AMPK. Additionally, we observed an enhanced expression of FOXO1. However, LCA did not induce the expression of NRF1 or PGC-1β in the *in vivo* setting.

We subsequently investigated the potential (patho)physiological relevance of the induced metabolic regulators (NRF1, AMPK, PGCs) in humans. Previous studies have highlighted the antitumor activity of AMPK and FOXO1 in human subjects. Utilizing the kmplot.com database, we discovered that high expression of NRF1 in breast cancer tissue is associated with improved survival following diagnosis. Collectively, these findings suggest that the modulation of AMPK, FOXO1, PGC-1β, or NRF1 may hold (patho)physiological relevance in influencing the effects triggered by LCA in humans.

Identification of LCA receptors

Our next objective was to determine the specific receptor(s) responsible for mediating the effects induced by LCA. To achieve this, we employed pharmacological inhibitors targeting different LCA receptors to assess their involvement in the LCA-induced effects. MCF7 cells were treated with LCA in combination with either vehicle or pharmacological agents that block potential LCA receptors. We observed that CINPA1 (CAR antagonist), NF449 (Gsα-selective antagonist), and U73343 (phospholipase C inhibitor) effectively blocked the LCA-mediated reduction in cell proliferation, while other inhibitors showed no significant effect. NF449 and U73343 effectively blocked inhibitory effect of LCA on cell proliferation and EMT, whereas CINPA1 did not exhibit the same efficacy.

To provide direct evidence for the involvement of TGR5, since NF449 and U73343 are not TGR5-specific inhibitors but can block TGR5 signaling by inhibiting Gsα and phospholipase C, we transiently silenced TGR5 in MCF7 cells. Silencing TGR5 efficiently blocked the LCA-induced morphological changes of MCF7 cells and prevented the upregulation of mRNA expression of mitochondrial markers including CYTOCHROME C, ATP5G1, and NDUFB5, as well as markers of AMPK activation. Additionally, it is worth noting that in the concentrations of

LCA used in this study, the dynamical properties and microdomain organization of biomembranes remained unaltered. This was demonstrated by the observation that neither the diffusion constant (D) nor the confinement time (tD) of LCA was affected, even upon treatment with 100 μM LCA.

Identification of breast cancer cell modulating bacterial metabolites

Metabolite library construction

Bacterial metabolites affecting human metabolism were identified through an extensive literature search. To ensure accuracy, the identified metabolites were carefully curated to exclude any falsely identified compounds that are not produced by bacteria. The reference concentrations of these metabolites in serum were established by literature searches. A recent study revealed that the presence of a tumor influences gut motility by modulating beta-adrenerg receptors. Altered passage speed within the gastrointestinal (GI) tract is likely to affect the redox environment, suggesting potential changes in the redox state of redox-labile metabolites in breast cancer patients. Therefore, the redox partners of each metabolite (mannose – D-mannitol, TMA – TMAO, 1-butanol – butyric acid, ethylene glycol – glycolic acid, oxalic acid) were incorporated into the metabolite library, and their serum reference concentrations were established through a comprehensive literature search. However, no specific literature data was available for ethylene glycol, so the same concentrations as the known redox pairs were utilized as reference. For a comprehensive overview of the metabolites, their serum reference concentrations, treatment concentrations, and corresponding literature sources, please refer to **Table 5**.

Developing high throughput techniques to assess cell proliferation

In our previous investigations, we identified and characterized a group of bacterial metabolites exhibiting cytostatic activity. However, the antiproliferative effects of these metabolites were limited, and the SRB proliferation assay did not prove highly precise data within that concentration range. To address this limitation, we evaluated two alternative methods for nucleus counting, based on image analysis. One method involved image segmentation and nucleus counting using CellProfiler, while the other utilized a deep learning (DL)-based method developed specifically for this project for segmentation, with nucleus counting performed using CellProfiler. The SRB assay provided unreliable at low cell densities in a range of 100-300 cells per well. Additionally,

the inherent limitations of photometry rendered values above an absorbance of 1.0 unreliable, restricting the maximum number of cells measurable at the end of an assay to 10 000 – 30 000. Values exceeding absorbance of 1.0 could be measured following dilution, introducing the possibility of dilution errors. In contrast, the image analysis-based assays exhibited a wider dynamic range compared to the SRB assay. Both analysis-based methods provided reliable results even at low cell numbers. Moreover, these assays were capable of detecting cell numbers up to 100 000 cells per well, with the DL-based method demonstrating superiority over CellProfiler's built-in method. Furthermore, the trained semantic segmentation models used in the DL-based method did not require parameter adjustment for every run, unlike conventional methods, offering an additional simplicity and increased accuracy between experiments for this segmentation approach. It is worth noting that the image analysis-based assays consistently yielded lower cell counts than the initially plated numbers when the cell densities ranged from 1 000 to 10 000. Upon visual inspection of these wells, it became apparent that cells adhered less to the plates at these densities, resulting in reduced cell numbers in the wells. This decrease in cell count observed in the culture plates confirmed the precision of the image analysis-based assays. Based on these findings, in subsequent experiments, we exclusively employed the image analysis-based methods.

Identifying microbial metabolites with pro- or antiproliferative properties

We evaluated the impact of the bacterial metabolites in our library on cell proliferation in 4T1 breast cancer cells. Cells were exposed to five different concentrations of each metabolite, covering the range of reference concentrations provided in. Statistical analysis was conducted independently for each metabolite's dose-response curve. Our findings revealed eight bioactive metabolites changing cell proliferation: butyric acid, glycolic acid, D-mannitol, 2,3-butanediol, trans-ferulic acid, 4-hydroxybenzoic acid, vanillic acid, and 3-hydroxyphenylacetic acid. Notably, formic acid exhibited antiproliferative properties at the highest concentration tested; however, we considered this observation cautiously as the highest concentration significantly exceeded the upper limit of the reference range. Butyric acid, glycolic acid, D-mannitol, 2,3-butanediol, and trans-ferulic acid demonstrated antiproliferative effects at the highest concentration employed, while 4-hydroxybenzoic acid, vanillic acid, and 3-hydroxyphenylacetic acid exhibited supportive effects on proliferation at specific concentrations.

Development of a high-throughput approach for evaluating EMT.

The bacterial metabolites previously identified in breast cancer, such as lithocholic acid, cadaverine, indole-derivatives, and short chain fatty acids, we found to impact epithelial-mesenchymal transition (EMT). To explore the potential modulation of EMT by the metabolite library, we employed a high-content image analysis methodology based on the observation that EMT alters cellular morphology in breast cancer. Additionally, we validated the results by assessing the protein-level expression of a set of EMT markers, such as vimentin and Snail. To establish positive and negative controls for EMT induction and inhibition, respectively, we applied transforming growth factor β 1 (TGF-β1) at a final concentration of 10 ng/mL, and SB-431542 at a final concentration of 2 μM, which is an inhibitor of TGF-β superfamily type I activin receptor-like kinases. The cells were treated with these compounds for 48 hours. Protein markers associated with mesenchymal transition, such as Zinc finger protein SNAI1 (Snail) and vimentin, were found to increase upon TGF-β1 induction, while vimentin, but not Snail was suppressed upon SB-431542 treatment in 4T1 cells. Furthermore, visual inspection of the cells confirmed the TGF-β-induced mesenchymal transition and the SB-431542 mediated epithelial transition. Consistent with these observations, high-content screening-based cell classification method indicated an increase in proportions of mesenchymal cells upon TGF-β1 induction, and a decrease in the proportions of mesenchymal cells following treatment with SB-431542. Based on these findings, we concluded that the high-content screening-based methods are reliable for determining the proportions of epithelial and mesenchymal cells under these experimental conditions.

Identifying bacterial metabolites affecting EMT

Following the validation of the developed method, we conducted an assessment of the metabolite library to determine their impact on EMT utilizing high-content screening. In this analysis, we identified 3-hydroxyphenylacetic acid, hydrocinnamic acid, 2,3-butanediol, and 4-hydroxybenzoic acid as compounds of interest. Notably, we observed a distinct V-shaped curve where an optimal concentration of each compound significantly reduced the proportion of mesenchymal cells, while lower and higher concentrations were ineffective. To validate these findings, we performed Western blot analysis. 4T1 cells were treated with the effective concentrations of the metabolites for 48 hours, and protein extracts were probed with anti-Snail and vimentin antibodies. With the exception of 2,3-butanediol, all metabolites exhibited a

reduction in the expression of at least one mesenchymal marker, confirming the results obtained from the high-content screening method. In the case of 2,3-butanediol, a decrease in the expression of EMT markers was observed but statistical tests did not reveal significant difference.

Discussion

The human body hosts a complex ecosystem of microorganisms, collectively known as the microbiome, which plays a crucial role in various physiological processes. The normal composition of the microbiome varies significantly from person to person, and defining the exact composition of the healthy microbiome is a challenging task. However, imbalance (dysbiosis) in the gut microbiome composition is linked to several intestinal and extra-intestinal diseases, e.g.: irritable bowel syndrome, coeliac disease, allergy, asthma, cardiovascular diseases, and obesity. In the last decade, dysbiosis was also linked to breast cancer. In breast cancer, the microbiome's composition undergoes significant changes, and becomes less diverse in the early stage. The exact cause of dysbiosis, and the pathomechanisms between breast cancer and the microbiome is still unknown. However, microbial metabolites reaching breast tissues affect cancer cells. Among the blood-transported bacterial metabolites, cadaverine, indoxyl sulfate, and indolepropionic acid were identified as antineoplastic agents in in breast cancer, in serum concentration range.

The effects of LCA in breast cancer

Earlier studies have suggested possible oncogenic properties of secondary bile acids. For instance, LCA demonstrated transforming capacity towards colon epithelial cells, while DCA (inactive in our model systems) was found to reprogram the secretome and promote hepatocellular carcinoma. Furthermore, DCA induced antineoplastic effects in pancreateic adenocarcinoma cells by inhibiting EMT, reducing cancer stemness. Additionally, bile acids have been implicated in pharyngeal cancer.

LCA is synthesized from primary bile acids by the gut microbiome and then reabsorbed at the terminal ileum, entering the enterohepatic circulation. Most of the LCA is then reabsorbed by the liver, but a small portion of it reaches remote parts of the body. In our experiments, LCA reduced the proliferation of MCF7, 4T1 and SKBR3 breast cancer cell lines. DCA and UDCA did not affect cell proliferation. These results were confirmed by SRB and colony forming assays. The effect was specific to breast cancer cell lines, as the primary fibroblast cell proliferation remained unchanged upon LCA treatment.

Changes in the total protein content or the colony size during the proliferation experiments could also be attributed to cell death. Previous studies reported that LCA can induce cell death in

neuroblastoma, prostate cancer, and MCF7 cells. However, the concentrations used in those studies were much higher than the serum concentrations we used during the experiments, which may account the absence of acute cytotoxicity. Our experiments showed, that propidium iodide cell number remained unchanged in treatments with physiological LCA concentrations, cell death was not the primary cause of change in the proliferation experiments.

LCA also reduced ratio of mesenchymal cell number in 4T1 breast cancer cell line. ECIS experiments also confirmed this observation in MCF7 and 4T1 cells, where the resistance values showed stronger cell-cell and cell-surface adhesion. Cell going through EMT have increased mobility, and weaker cell-cell connections. In scratch assays, we measured slower gap closure in 4T1 cell lines upon LCA treatment. Together these results show mesenchymal to epithelial transition (MET) upon LCA treatment.

β-catenin, an important transcription factor in the Wnt pathway, regulating cell proliferation in the G1 phase. In colorectal cancers, β-catenin also induces EMT and pro-invasion expression profiles through T-cell and lymphoid enhancer (TCF-LEF) factor activation. Conventionally, β-catenin level assessment requires the evaluation of pGSK-3α/β / GSK-3α/β levels, as phosphorylated GSK-3α/β promotes β-catenin degradation [68]. Our *in vitro* Western blot analysis revealed that β-catenin protein level decreased, while GSK-3α/β goes through dephosphorylation in MCF7 and 4T1 cell lines during LCA treatment. β-catenin levels can give an explanation for the proliferation changes in our experiments. GSK-3α/β signaling on the other hand seems to be disconnected from β-signaling. This can be explained in several ways, e.g.: mutations in growth signaling pathways, or alternative GSK-3α/β activation through PI3K/Akt, protein phosphatase2, or protein kinase B. β-catenin protein level was also decreased in our *in vivo* samples, in LCA treatment.

Our *In vivo* experiments showed, that tumor infiltrating lymphocyte number is increasing upon LCA treatment, while qPCR measurements showed decreased Vegfa mRNA in tumor samples. TIL number is a common prognostic marker in breast cancer, indicating better prognosis, while VEGFA is a vascularization marker.

We also wanted to assess the typical Warburg metabolism markers in the study. Generally, OCR and ECAR, oxidative phosphorylation gene (CytC, ATP5g1, NUDFB5) and energy metabolism regulator gene expression (FOXO1, PGC1-β, NRF1) and activity was increased upon LCA treatment both *in vitro* and in *in vivo* experiments. Pulse-chase metabolomic measurements showed a higher succinate/lactate and citrate/lactate level in MCF7 and 4T1 cell lines. These collectively indicate

increased activity of TCA cycle and oxidative phosphorylation upon LCA treatment. In other words, LCA treatment induced an anti-Warburg response in the breast cancer cells, providing a possible explanation for decreased cell proliferation.

LCA most likely affects cell signaling pathways through multiple receptors. In our experiments, part of the observed effects were most likely the result of TGR5 signaling, as specific inhibition of this receptor reverted back LCA-induced cell morphology and proliferation changes.

Standardization of microscopy image analysis

In this study, one of our aim was to create a standardized high throughput image analysis method, to measure cell proliferation and EMT in varying conditions via fluorescent microscopy. For this purpose, we applied conventional image analysis techniques and deep learning techniques.

The base of the deep learning model was a fine-tuned a VGG16 feature extraction model pretrained on ImageNet, joined with a U-Net segmentation model. VGG16 is broadly used for image classification, and pretrained weights are readily available for this model. U-Net is a general purpose segmentation model, commonly used in biomedical image analysis applications. After training, our fine-tuned nuclei segmentation model performed >98% accuracy on the validation dataset. The deep learning-coupled nuclei counting method analyzed more than 60 000 images without human interference and were comparable to conventional nuclei counting methods, where parameter adjustments were required for each independent dataset. This method outperforms conventional image analysis methods and SRB proliferation assay as well, showing higher accuracy in extreme low and high cell counts (100 – 100 000 cell/well).

The trained neural network is well-generalized for at least 4T1 nuclei segmentation tasks, and potentially well trained to segment other cell lines' nuclei included in the training set as well. Cancer cells however, could show nuclear pleomorphism, that may easily disrupt fine-tuned image analysis methods. Another problem is the time- and resource-consuming imaging and image analysis, compared to other well-established chemistry-based proliferation assays (as SRB-assay). An easy solution to these problems would be specifically including images of pleomorphism in the training dataset for the deep learning segmentation models, to train the model for amorphous nuclei segmentation as well. Furthermore, using exclusively brightfield images (no fluorescent labeling) for cell and nuclei segmentation could lead to drastically reduced cost and time of imaging/analysis without losing

significant accuracy. These principles can also be applied to develop a stand-alone automatized analytic method to measure breast cancer cell features, such as proliferation and EMT.

The role of bacterial metabolites in breast cancer

To date, the majority of bioactive bacterial metabolites discovered have shown anti-neoplastic properties. Additionally, in breast cancer patients, levels of enzymes involved in producing these bacterial metabolites have been found to decrease in the gut microbiome compared to healthy individuals.

In our research, we identified 9 bacterial metabolites that impact the proliferation and morphology of the 4T1 breast cancer cell line. Notably, formic acid significantly decreased cell proliferation. However, it's important to acknowledge that the concentration used in our study exceeds the upper limit of the physiological serum concentration range.

A recent study revealed the occurrence of ileopathy in various cancers, including breast cancer. Slower passage through the gastrointestinal tract not only changes the composition of the microbiome but also likely impacts the redox balance of the GI tract contents. Due to this observation, we also explored bacterial metabolites in redox pairs. Several redox pairs were identified within the short-chain fatty acid and polyol group (e.g., D-mannitol – D-mannose, 1-butanol – butyric acid, ethylene glycol – glycolic acid – oxalic acid), where only one partner displayed cytostatic properties. This finding suggests that altered redox environment may influence the metabolome/secretome in breast cancer.

The bacterial metabolites identified in our experiments belong to various chemical groups, necessitating separate discussions. D-mannose is a monosaccharide, and D-mannitol is a sugar alcohol or polyol. In our experiments, D-mannitol significantly reduced cell proliferation, whereas its redox pair, D-mannose, did not affect breast cancer cell proliferation. Literature shows, that mannitol is already a therapeutic target in cisplatin treated cancer patients due to its nephroprotective properties, although the concentration applied in that study (approximately 16 mM) is significantly higher than that of the highest concentration (128 μM) we used in our current research. Controversially, other studies appropriate mannitol nephrotoxic properties at high concentrations, in patients with renal failure. To date, D-mannitol was not studied in other cancer related research projects.

Another polyol, 2,3-butanediol is unique among the bacterial metabolites investigated in our research, due to its ability to inhibit both proliferation and EMT. It is also worth noting, that the ability to synthesize 2,3-butanediol is widespread among bacteria. According to these findings, 2,3-butanediol

could be the most promising candidate as an anti-neoplastic bacterial metabolite.

On the oxalic acid, glycolic acid, and ethylene glycol redox axis, we found that only one of these bacterial metabolites exhibited an effect on breast cancer cells. Glycolic acid, a short-chain fatty acid, significantly decreased cell proliferation. Similar to D-mannitol, glycolic acid has not been previously investigated in breast cancer. Apart from its physiological serum concentration range, the known information about glycolic acid pertains to its use in chemical peels and anti-acne formulations in dermatology.

Butyric acid, another short-chain fatty acid, has demonstrated antiproliferative properties in our experiments. Butyric acid affects breast cancer cells through various mechanisms, serving as an inhibitor of histone deacetylases (an epigenetic modifier), a metabolic substrate, and a ligand to free fatty acid receptors. Notably, butyric acid levels were found to decrease in the feces of breast cancer patients.

Trans-ferulic acid, a polyphenol, reduced cell proliferation. Literature indicates, that ferulic acid, a potentially anti-tumor microbial metabolite, inhibits breast cancer cell proliferation, promotes apoptosis, and reduce migration speed *in vitro* within the range of 10-100 μM. Recent studies suggest that it may also inhibit breast cancer formation. It is important to note that the molecule investigated in our experiments is the trans isoform of ferulic acid, and our findings should be interpreted accordingly.

4-hydroxybenzoic acid is synthesized from chorismic acid and can bind to the estrogen receptor, peroxisome proliferator activated receptor (PPAR)γ and G-protein-coupled receptor 40 (GPR40). 4-hydroxybenzoic acid treatment increased cell proliferation, while inhibited EMT.

Vanillic acid belongs to the benzoic acid chemical class. In our experiments, vanillic acid significantly increased cell proliferation. Notably, trans-ferulic acid and vanillic acid are present in the extracts of bacteria or plants tested for their anticancer potential. Furthermore, vanillic acid has been shown to act as pro-oxidant and suppress cell proliferation.

Lastly, among the polyphenols, 3-hydroxyphenylacetic acid reduced cell proliferation, furthermore both hydrocinnamic acid and 3-hydroxyphenylacetic acid inhibited EMT. Compounds such as hydrocinnamic acid, 3-hydroxyphenylacetic acid, and 4-hydroxyphenylacetic acid comprise an aromatic ring and a polar carboxylic and moiety. Hydrocinnamic acid has been demonstrated to be a product of lactic acid-producing bacteria. On the other hand, 3-hydroxyphenylacetic acid is a flavonoid compound generated through the degradation of quercetin-derivatives, which are synthesized by the human microbiome, partly by *Clostridiales*. Notably, 3-hydroxyphenylacetic acid exhibits

cytoprotective features and can bind to the γ-hydroxybutirate receptor.

Several metabolites identified in this study, such as glycolic acid, hydrocinnamic acid, 2,3-butanediol, 3-hydroxyphenylacetic acid, and 4-hydroxyphenylacetic acid, have been shown to have antibacterial activity or are involved in quorum sensing. This suggests that these metabolites may not only affect breast tumor cells but also influence the microbiome.

In our experiments, we have seen a V-shaped or inverted V-shaped dose-response curve in several cases (e.g. 2,3-butanediol/EMT, 4-hydroxybenzoic acid/proliferation). This behavior is similar to certain previously identified antineoplastic bacterial metabolites, such as indoxyl-sulfate or indolepropionic acid (in both cases, V-shape was observed). An inverted V-shaped curve suggests a sequence of events where a receptor is initially stimulated, promoting proliferation at low concentrations, and then another receptor becomes activated, inhibiting proliferation at higher concentrations. It's worth noting that although toxicity can sometimes show similar patterns at high concentrations, in this study, the compounds were kept within the recommended range, reducing the likelihood of a toxic effect.

Summary

There is a strong connection between the microbiome and the host. Bacteria residing in various parts of the human body generate a multitude of bacterial metabolites, which have the ability to impact the host. Vice versa, the host – through diet, personal hygiene, genetics, and age – can also affect the composition and function of the microbiome. Changes in the microbiome's composition or function are linked to several diseases, including breast cancer.

Lithocholic acid (LCA), a secondary bile acid, which is produced by bacteria coding the baiH ORF. LCA reaches breast cancer cells through the bloodstream located distantly from the gut microbiome. LCA reduced the proliferation and colony formation ability of MCF7, 4T1 and SKBR3 breast cancer cells, inhibited the epithelial-mesenchymal transition (EMT), and shifted energy metabolism toward oxidative phosphorylation, hence, reverting the Warburg effect in cultured cells. LCA also inhibits cell migration while promoting cell-to-cell and cell-to-surface connections. LCA supplementation in mice increases the number of tumor-infiltrating lymphocytes in the primary tumor. LCA elicited its effects through the TGR5 receptor, as inhibiting or silencing this receptor prevents LCA-induced EMT and the expression of LCA-induced genes (pACC, ATP5G1, and NDFUB5).

The study also evaluated a carefully curated library of 30 other bacterial metabolites and applied these in their serum reference concentrations in cellular models. Nine of these metabolites were found to be bioactive. Butyric acid, glycolic acid, D-mannitol, 2,3-butanediol, and trans-ferulic acid were shown to reduce cell proliferation, while 4-hydroxybenzoic acid, vanillic acid, and 3-hydroxyphenylacetic acid increased cell proliferation. Among these metabolites, 4-hydroxybenzoic acid, 2,3-butanediol, hydrocinnamic acid, and 3-hydroxyphenylacetic acid were found to significantly inhibit, while no metabolite increased EMT.

In conclusion, the study suggests that LCA can suppress key features of breast cancer cells, potentially exerting a control over carcinogenesis. Furthermore, the newly discovered bioactive metabolites may also have a similar effect. However, more extensive research is required to firmly establish the role of these metabolites in breast cancer.

Összefoglalás

A mikrobiom és a gazdaszervezet között kétirányú kapcsolat áll fenn. A baktériumok – melyek az emberi szervezet különböző testüregeiben élnek – számos metabolitot termelnek, melyek befolyásolhatják a gazdaszervezet metabolizmusát és energia háztartását. Külső és belső tényezők (étrend, személyes higiénia, genetika, életkor) által a gazdaszervezet is befolyásolja a mikrobiom összetételét és működését. Számos betegség, köztük az emlődaganat is összefüggésbe hozható a mikrobiom összetételében és működésében bekövetkező változásokkal.

A litokólsav (LCA), egy másodlagos epesav, melyet a baiH ORF-et kódoló baktériumok állítanak elő. Az LCA a véráram útján a test távoli pontjaiba is eljut, így az emlődaganat szövetekhez is. Kísérleteinkben az LCA gátolta a sejtosztódást és a kolóniaformálási kapacitást MCF7, 4T1 és SKBR3 sejtekben, valamint gátolta az epithelialis-mesenchymalis tranzíciót, a sejt energia-anyagcseréjét az oxidatív foszforiláció irányába változtatta, tehát anti-Warburg hatást mutatott a sejtkultúrákban. Az LCA gátolta a sejt migrációt és elősegítette a sejt-sejt és sejt-felszín kapcsolatokat. Primer tumorokban LCA hatására a tumor-infiltráló limfociták száma megnőtt. A kísérletek azt mutatják, hogy az LCA ezen hatásait a TGR5 receptoron keresztül fejti ki, mivel a receptor gátlásával vagy csendesítésével az LCA-indukált EMT és az EMT-re jellemző gének kifejeződése (pACC, ATP5G1, NDUFB5) gátolt.

A tanulmányban továbbá megvizsgáltuk az általunk válogatott bakteriális metabolit könyvtár tagjainak hatását. Ezeknek a bakteriális metabolitoknak ismert a fiziológiás szérum koncentrációja. A könyvtárból kilenc metabolit bizonyult bioaktívnak. A butirát, glikolát, D-mannitol, 2,3-butándiol és transz-ferulát csökkentette, míg a 4-hidroxibenzoát, vanilinsav, 3-hidroxiphenilacetát elősegítette a sejtproliferációt. A metabolitok közül a 4-hidroxibenzoát, 2,3-butándiol, hidrocinnamonsav és 3-hidroxifenilacetát szignifikánsan gátolta az EMT-t és nem találtunk olyan metabolitot, mely elősegítette volna.

Jelen disszertáció alapján az LCA gátolja az emlőtumoros sejtek főbb jellemzőit, potenciálisan befolyásolja a karcinogenezist. Továbbá, az újonnan felfedezett bioaktív metabolitoknak hasonló tulajdonságaik lehetnek. Azonban ez a terület további kutatásokat igényel, hogy igazoljuk ezeket a hatásokat.

Keywords

Lithocholic acid, breast cancer, bacterial metabolites, EMT, semantic segmentation

UNIVERSITY of DEBRECEN

UNIVERSITY AND NATIONAL LIBRARY
UNIVERSITY OF DEBRECEN
H-4002 Egyetem tér 1, Debrecen
Phone: +3652/410-443, email: publikaciok@lib.unideb.hu

Registry number: DEENK/448/2023.PL
Subject: PhD Publication List

Candidate: Gyula Ujlaki
Doctoral School: Doctoral School of Molecular Medicine

List of publications related to the dissertation

1. **Ujlaki, G.**, Kovács, T., Vida, A., Kókai, E., Rauch, B., Schwarcz, S., Mikó, E., Janka, E. A., Sipos, A., Hegedűs, C., Uray, K., Nagy, P., Bai, P.: Identification of bacterial metabolites modulating breast cancer cell proliferation and epithelial-mesenchymal transition.
   Molecules. 28 (15), 1-18, 2023.
   DOI: http://dx.doi.org/10.3390/molecules28155898
   IF: 4.6 (2022)
2. Mikó, E., Vida, A., Kovács, T., **Ujlaki, G.**, Trencsényi, G., Márton, J., Sári, Z., Kovács, P., Boratkó, A., Hujber, Z., Csonka, T., Antal-Szalmás, P., Watanabe, M., Gombos, I., Csóka, B., Kiss, B. K., Vígh, L., Szabó, J., Méhes, G., Sebestyén, A., Goedert, J. J., Bai, P.: Lithocholic acid, a bacterial metabolite reduces breast cancer cell proliferation and aggressiveness.
   Biochim. Biophys. Acta Bioenerg. 1859 (9), 958-974, 2018.
   DOI: http://dx.doi.org/10.1016/j.bbabio.2018.04.002
   IF: 4.441

List of other publications

3. Skopál, A., **Ujlaki, G.**, Gerencsér, A., Bankó, C., Bacsó, Z., Ciruela, F., Virág, L., Haskó, G., Kókai, E.: Adenosine A2A Receptor Activation Regulates Niemann-Pick C1 Expression and Localization in Macrophages.
   Curr. Issues Mol. Biol. 45 (6), 4948-4969, 2023.
   DOI: http://dx.doi.org/10.3390/cimb45060315
   IF: 3.1 (2022)
4. Antal, D., Pór, Á., Kovács, I., Dull, K., Póliska, S., **Ujlaki, G.**, Demény, M. Á., Szöllősi, A. G., Kiss, B. K., Szegedi, A., Bai, P., Szántó, M.: PARP2 promotes inflammation in psoriasis by modulating estradiol biosynthesis in keratinocytes.
   J. Mol. Med. (Berl). 101 (8), 987-999, 2023.
   DOI: http://dx.doi.org/10.1007/s00109-023-02338-z
   IF: 4.7 (2022)

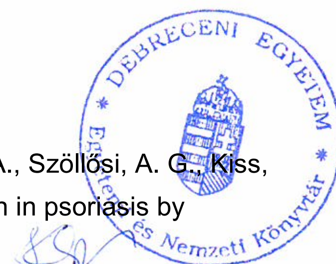

UNIVERSITY AND NATIONAL LIBRARY
UNIVERSITY OF DEBRECEN
H-4002 Egyetem tér 1, Debrecen
Phone: +3652/410-443, email: publikaciok@lib.unideb.hu

5. Schwarcz, S., Kovács, P., Kovács, T., **Ujlaki, G.**, Nyerges, P., Uray, K., Bai, P., Mikó, E.: The pro- and antineoplastic effects of deoxycholic acid in pancreatic adenocarcinoma cell models.
   Mol. Biol. Rep. 50 (6), 5273-5282, 2023.
   DOI: http://dx.doi.org/10.1007/s11033-023-08453-x
   IF: 2.8 (2022)

6. Lénárt, K., Bankó, C., **Ujlaki, G.**, Póliska, S., Kis, G., Csősz, É., Antal, M., Bacsó, Z., Bai, P., Fésüs, L., Mádi, A.: Tissue Transglutaminase Knock-Out Preadipocytes and Beige Cells of Epididymal Fat Origin Possess Decreased Mitochondrial Functions Required for Thermogenesis.
   Int. J. Mol. Sci. 23 (9), 5175, 2022.
   DOI: http://dx.doi.org/10.3390/ijms23095175
   IF: 5.6

7. Kiss, B. K., Mikó, E., Sebő, É., Tóth, J., **Ujlaki, G.**, Szabó, J., Uray, K., Bai, P., Árkosy, P.: Onkobiózis és mikrobiális metabolikus jelátvitel pancreas-adenocarcinomában.
   Cent. Eur. J. Gastro. Hepatol. 7 (2), 57-65, 2021.
   DOI: http://dx.doi.org/10.33570/CEUJGH.7.2.57

8. Kacsir, I., Sipos, A., **Ujlaki, G.**, Buglyó, P., Somsák, L., Bai, P., Bokor, É.: Ruthenium half-sandwich type complexes with bidentate monosaccharide ligands show antineoplastic activity in ovarian cancer cell models through reactive oxygen species production.
   Int. J. Mol. Sci. 221, 1-41, 2021.
   DOI: http://dx.doi.org/10.3390/ijms221910454
   IF: 6.208

9. Jankó, L., Kovács, T., Laczik, M., Sári, Z., **Ujlaki, G.**, Kis, G., Horváth, I., Antal, M., Vígh, L., Bálint, B. L., Uray, K., Bai, P.: Silencing of Poly(ADP-Ribose) Polymerase-2 Induces Mitochondrial Reactive Species Production and Mitochondrial Fragmentation.
   Cells. 10 (6), 1387, 2021.
   DOI: http://dx.doi.org/10.3390/cells10061387
   IF: 7.666

10. Kovács, T., Mikó, E., **Ujlaki, G.**, Mustafa, H. Y. H., Csontos, V., Uray, K., Bai, P.: The involvement of oncobiosis and bacterial metabolite signaling in metastasis formation in breast cancer.
   Cancer Metastasis Rev. 40, 1223-1249, 2021.
   DOI: http://dx.doi.org/10.1007/s10555-021-10013-3
   IF: 9.237

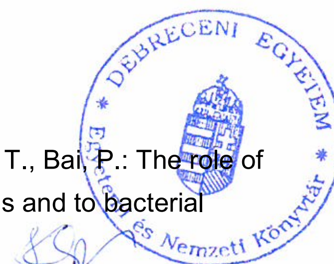
DEBRECENI EGYETEM
Egyetemi és Nemzeti Könyvtár

11. Sipos, A., **Ujlaki, G.**, Mikó, E., Maka, E., Szabó, J., Uray, K., Krasznai, Z. T., Bai, P.: The role of the microbiome in ovarian cancer: mechanistic insights into oncobiosis and to bacterial metabolite signaling.
   Mol. Med. 27 (1), 1-20, 2021.
   DOI: http://dx.doi.org/10.1186/s10020-021-00295-2
   IF: 6.376

12. Sári, Z., Mikó, E., Kovács, T., Jankó, L., Csonka, T., Lente, G., Sebő, É., Tóth, J., Tóth, D., Árkosy, P., Boratkó, A., **Ujlaki, G.**, Török, M., Kovács, I., Szabó, J., Kiss, B. K., Méhes, G., Goedert, J. J., Bai, P.: Indolepropionic Acid, a Metabolite of the Microbiome, Has Cytostatic Properties in Breast Cancer by Activating AHR and PXR Receptors and Inducing Oxidative Stress.
    Cancers (Basel). 12 (9), 1-27, 2020.
    DOI: http://dx.doi.org/10.3390/cancers12092411
    IF: 6.639

13. Sári, Z., Mikó, E., Kovács, T., Boratkó, A., **Ujlaki, G.**, Jankó, L., Kiss, B. K., Uray, K., Bai, P.: Indoxylsulfate, a Metabolite of the Microbiome, Has Cytostatic Effects in Breast Cancer via Activation of AHR and PXR Receptors and Induction of Oxidative Stress.
    Cancers (Basel). 12 (10), 1-23, 2020.
    DOI: http://dx.doi.org/10.3390/cancers12102915
    IF: 6.639

14. Kiss, B. K., Mikó, E., Sebő, É., Tóth, J., **Ujlaki, G.**, Szabó, J., Uray, K., Bai, P., Árkosy, P.: Oncobiosis and microbial metabolite signaling in pancreatic adenocarcinoma.
    Cancers (Basel). 12 (5), 1-34, 2020.
    DOI: http://dx.doi.org/10.3390/cancers12051068
    IF: 6.639

15. Kovács, T., Mikó, E., **Ujlaki, G.**, Sári, Z., Bai, P.: The Microbiome as a Component of the Tumor Microenvironment.
    In: Tumor Microenvironment / Alexander Birbrair, Springer Nature - Springer Cham, Switzerland, 137-153, 2020, (dvances in Experimental Medicine and Biology, 0065-2598 ; 1225)

16. Kovács, T., Mikó, E., Vida, A., Sebő, É., Tóth, J., Csonka, T., Boratkó, A., **Ujlaki, G.**, Lente, G., Kovács, P., Tóth, D., Árkosy, P., Kiss, B. K., Méhes, G., Goedert, J. J., Bai, P.: Cadaverine, a metabolite of the microbiome, reduces breast cancer aggressiveness through trace amino acid receptors.
    Sci Rep. 9 (1), 1-14, 2019.
    DOI: http://dx.doi.org/10.1038/s41598-018-37664-7
    IF: 3.998

17. Kovács, P., Csonka, T., Kovács, T., Sári, Z., **Ujlaki, G.**, Sipos, A., Karányi, Z., Szeőcs, D., Hegedűs, C., Uray, K., Jankó, L., Kiss, M., Kiss, B. K., Laoui, D., Virág, L., Méhes, G., Bai, P., Mikó, E.: Lithocholic acid, a metabolite of the microbiome, increases oxidative stress in breast cancer.
    Cancers (Basel). 11, 1-31, 2019.
    DOI: http://dx.doi.org/10.3390/cancers11091255
    IF: 6.126

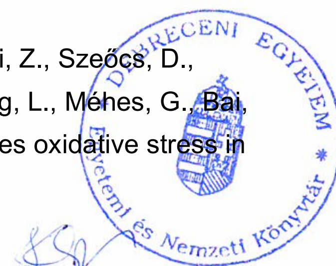

UNIVERSITY AND NATIONAL LIBRARY
UNIVERSITY OF DEBRECEN
H-4002 Egyetem tér 1, Debrecen
Phone: +3652/410-443, email: publikaciok@lib.unideb.hu

18. Mikó, E., Kovács, T., Sebő, É., Tóth, J., Csonka, T., **Ujlaki, G.**, Sipos, A., Szabó, J., Méhes, G., Bai, P.: Microbiome-Microbial Metabolome-Cancer Cell Interactions in Breast Cancer-Familiar, but Unexplored.
    Cells. 8 (4), 1-33, 2019.
    DOI: http://dx.doi.org/10.3390/cells8040293
    IF: 4.366

19. Nagy, L., Rauch, B., Balla, N., **Ujlaki, G.**, Kis, G., Omar, A. R., Kristóf, E., Sipos, A., Antal, M., Tóth, A., Debreceni, T., Horváth, A., Maros, T. M., Csizmadia, P., Szerafin, T., Bai, P.: Olaparib induces browning of in vitro cultures of human primary white adipocytes.
    Biochem. Pharmacol. 167, 76-85, 2019.
    DOI: http://dx.doi.org/10.1016/j.bcp.2019.06.022
    IF: 4.96

Total IF of journals (all publications): 94,095
Total IF of journals (publications related to the dissertation): 9,041

The Candidate's publication data submitted to the iDEa Tudóstér have been validated by DEENK on the basis of the Journal Citation Report (Impact Factor) database.

02 October, 2023